JOURNAL OF GEOPHYSICAL RESEARCH, VOL. 102, NO. B7, PAGES 14,821–14,833, JULY 10, 1997

Three-dimensional flow and reaction in porous media: Implications for the Earth's mantle and sedimentary basins

E. Aharonov and M. Spiegelman
Lamont-Doherty Earth Observatory of Columbia University, Palisades, New York

P. Kelemen
Woods Hole Oceanographic Institution, Woods Hole, Massachusetts

Abstract. We present a theoretical and numerical study of the reorganization of a porous matrix due to fluid flow coupled with dissolution or precipitation processes. We find that under certain conditions, flow of corrosive fluids results in unstable growth of the permeability and increasing disequilibrium in fluid chemistry with time. High-permeability channels may form parallel to the direction of flow. In time, these channels cause the distribution of porosity to become increasingly correlated and anisotropic and cause flow rates to be increasingly variable. Flow coupled with crystallization has the opposite effect: With time, permeability reduction occurs at a decreasing rate. Mineral composition in the fluid approaches chemical equilibrium. Precipitation destroys existing preferred paths for flow and acts to homogenize and disperse the flow. Connectivity of the porous media is reduced. Implications of these results for two geological systems are discussed: (1) Modes of melt extraction from the Earth's mantle, where the expected different modes of flow and reaction may help explain different geochemical and geological observations at hot spots and mid-ocean ridges, and (2) Precipitation and formation of abnormal pressure zones in sedimentary basins.

Introduction

Understanding coupled flow and reaction is important in a variety of geological and industrial settings. Dissolution and precipitation that occur during fluid flow are responsible, to a large degree, for the formation of sedimentary rocks from the initial unconsolidated sediments [*Richardson and McSween*, 1989]. The flow patterns and chemistry within the Earth's mantle are also affected by processes of reactive porous flow [e.g., *Boudier and Nicolas*, 1977; *Dick*, 1977; *Quick*, 1981; *Bodinier*, 1988; *Kelemen et al.*, 1992, 1995a; *Ozawa*, 1994], but here the fluid is magma, and the range of temperatures is much higher. Geologists, hydrologists, oil companies, companies concerned with environmental restoration, and even coffee percolator manufacturers would like to understand and quantify the time dependent changes in the properties of porous media due to clogging or corroding processes. As will be demonstrated in this paper, fluid flow coupled with chemical reactions induces long-range interactions, disequilibrium, and substantial changes in the solid geometry.

The coupled fluid-solid dynamical system may be studied via different approaches, ranging from microscopic studies [*Wells et al.*, 1991; *Kelemen et al.*, 1995a; *Bekri et al.*, 1995] of reactive "particles" in actual "pores," to analog network simulations [*Hoefner and Fogler*, 1988], to solutions of macroscopic partial differential equations [*Chadam et al.*, 1986; *Ortoleva et al.*, 1987; *Steefel and Lasaga*, 1994; *Aharonov et al.*, 1995]. In this paper, we present an initial numerical and theoretical study of the coupled system of flow and reaction in porous media, using a set of partial differential equations which are applicable above the Darcy scale. Our three-dimensional numerical model is similar in concept to the model implemented by *Steefel and Lasaga* [1994] but is introduced and used here in a simplified form in order to focus on the basic physical processes that control reactive flow in porous media. We aim to quantify the evolving nature and statistics of reacting porous media and to establish the different effects of dissolution and precipitation on the morphology of the matrix and the evolution of transport properties.

In general, the process of reactive flow (and especially flow coupled with precipitation) has not been studied extensively. Many of the existing quantitative studies have focused on the stability of a propagating dissolution front. A dissolution front is a transient phenomenon, where an undersaturated fluid is injected at one end of the porous media and emerges partially or fully equilibrated at the other end after it has reacted with the porous media. The width of the front marks the reaction zone. The position of the front may undergo a fingering instability termed the "reactive infiltration instability." The reactive-infiltration instability is observed in both two-dimensional and 3-D laboratory experiments [*Hoefner and Fogler*, 1988; *Daccord and Lenormand*, 1987]. Some numerical simulations and analytical predictions exist for the 2-D reactive infiltration instability [e.g., *Chadam et al.*, 1986; *Steefel and Lasaga*, 1990]. The form of this instability in three dimensions is yet to be fully understood.

Paper number 97JB00996.
0148-0227/97/97JB-00996$09.00

Although reaction fronts are found in geological systems, they represent a "special event" which causes disequilibrium, like the intrusion of a magmatic body. A possibly more common form of reaction emerges spontaneously, even in initially equilibrated systems, because of flow along an imposed gradient in mineral solubility [*Phillips*, 1991]. Flow in geological systems is often induced by temperature and pressure gradients, and since solubility in many minerals is a function of temperature and pressure, fluids will experience a solubility gradient along the flow path. An example of such a system is a sedimentary basin which is actively compacting, where aqueous fluids may become increasingly supersaturated in minerals (e.g., clays) as they upwell and cool. Another example is the Earth's upper mantle which is upwelling beneath mid-ocean ridges. In this case, melt rises, decompresses, and becomes increasingly undersaturated in pyroxene [e.g., *Sleep*, 1975; *Kelemen et al.*, 1995a]. In such cases, even if the system is initially in equilibrium, the existence of flow will induce continuous reaction. Gradient systems are thus appealing not only because of their geological applicability but also because they provide a nontransient generic setting for the study of coupled flow and reaction, where reaction occurs continuously everywhere, rather than only along a finite reaction front. This paper concentrates on studying such gradient systems.

The outline of the paper is as follows. In the first section we propose a set of partial differential equations that macroscopically describe reactive flow through a porous media. In the second section the general setting of the study is presented, and some simplified, first-order predictions for the average behavior of the system are presented. In the third section the numerical method used to solve these equations is detailed, and simulation conditions are described. In the fourth section results of the dissolution and precipitation simulations are presented, and their average behavior is compared to the theoretical predictions. Morphology and statistical properties of dissolving and precipitating media are contrasted with one another and compared to those of the initially random media. We find that dissolution can lead to unstable growth of organized high-permeability channels in the direction parallel to flow, whereas precipitation tends to destroy preferred paths for flow. Combined systems, where the fluid first flows through a region where it is corrosive to the porous matrix and then through a region of precipitation, produce overpressure at the transition from dissolution to precipitation. We conclude the paper by discussing the relevance of this work to two geological systems: melt extraction from the Earth's mantle and formation of abnormal pressure zones in sedimentary basins.

Formulation of the Problem

The description derived below is similar to that given by *Chadam et al.* [1986]; *Steefel and Lasaga* [1990], and *Aharonov et al.* [1995]. The mathematical formalism uses a conventional continuum approach suited for description of flow through a rigid porous matrix at and above the Darcy scale (the scale of a few pores), where one can define smoothly varying porosity and permeability. It was shown previously by linear analysis [*Aharonov et al.*, 1995] that addition of compaction does not inhibit unstable formation of channels during dissolution, but the full effect of adding solid compaction [e.g., *Spiegelman*, 1993] and addition of explicit temperature will be discussed in a different paper (M. Spiegelman *et al.*, manuscript in preparation, 1997).

General Equations

Mass conservation. The mass conservation equations are

$$\frac{\partial \rho_s(1-\phi)}{\partial t} = \sum_i \Gamma_i, \tag{1}$$

$$\frac{\partial \rho_f \phi}{\partial t} + \nabla \cdot (\rho_f \mathbf{v} \phi) = -\sum_i \Gamma_i, \tag{2}$$

$$\frac{\partial \rho_s(1-\phi)c_i^s}{\partial t} = \nabla \cdot [D_i^s \rho_s (1-\phi) \nabla c_i^s] + \Gamma_i, \tag{3}$$

$$\frac{\partial \rho_f \phi c_i}{\partial t} + \nabla \cdot (\rho_f \phi \mathbf{v} c_i) = \nabla \cdot [\mathbf{D}_i \rho_f \phi \nabla c_i] - \Gamma_i, \tag{4}$$

where ϕ is the porosity, ρ_s and ρ_f are the solid and fluid density, respectively, in kg m^{-3}, and Γ_i is the net mass transfer rate of component i from fluid to solid in kg m^{-3} s^{-1}. For general multicomponent systems of M mineral phases present in the rock, $\Gamma_i = \sum_1^M \nu_{im} \mathcal{R}_m$, where ν_{im} is the stoichiometric proportion of component i in mineral m and $\mathcal{R}_m$ is the dissolution or precipitation rate of mineral m in units of kg m^{-3} s^{-1}. For a review of general analytical formulation of dissolution and precipitation in multicomponent systems, see *Steefel and Lasaga* [1994]. $\mathbf{v}$ is the fluid velocity vector in m s^{-1}, t is time, and D_i^s is the diffusion coefficient of component i within the solid. The dispersion tensor $\mathbf{D}_i$ is the sum of mechanical dispersion of flow and molecular diffusion within the fluid [*Bear*, 1972]. Variables c_i and c_i^s are the mass fractions of component i in the fluid and solid, respectively, with $\sum_i c_i = 1$ and $\sum_i c_i^s = 1$.

Equations (1) and (2) describe the conservation of total solid and fluid mass, respectively. Equations (3) and (4) describe the conservation of each mineral component in the solid and fluid phase, respectively.

Flow through porous media. The closing equation is Darcy's law, which relates a driving pressure p to the flux of the fluid:

$$\phi \mathbf{v} = -\frac{k}{\mu} \nabla p, \tag{5}$$

where μ is the viscosity of the fluid and k is the permeability. It can be shown that for a rigid medium, with a uniform gravitational body force, the driving pressure gradients can be written as

$$\nabla p = \nabla p_e + (\rho_s - \rho_f)\mathbf{g}, \tag{6}$$

when $\phi \ll 1$ and fluid and solid densities are constant. Equation (6) states that under the above approximations the pressure gradient can be decomposed into a constant background gradient driven by the buoyancy difference between the fluid and the solid and an excess pressure p_e.

The relation between the permeability and the geometry of the matrix is important for realistically modeling nonlinear processes involved in this study, but a clear analytical description is not obvious. For example, it is possible that by selective precipitation (or dissolution) in strategically positioned necks the porosity will be hardly changed, while the permeability will be highly altered. Nevertheless, permeability is commonly assumed to be a power law function of the porosity [e.g., *Bear*, 1972]

$$k(\phi) = d^2\phi^n/b, \tag{7}$$

with d being a typical grain size, n usually greater or equal to 2, and b a constant. This relation is used here as a first, though not perfect, approximation. An improved permeability-porosity relation is suggested by *Aharonov et al.* [1997] but is not used here for simplicity.

Boundary conditions. In general, equations (1)-(7) will require either pressure or flux boundary conditions, as well as boundary conditions for each mineral component. Initial conditions on ϕ and c_i are also needed in order to determine the spatial and temporal evolution of $\mathbf{v}$, p, ϕ, c_i^s, and c_i.

Simplifications

Since we are interested in the basic effects of the coupled system of flow and reaction, we investigate the simplest system of a single soluble component ($c_i^s = 1$) which can chemically dissolve or precipitate by first-order linear kinetics. The fluid phase is thus composed of a carrier fluid with mass fraction $1 - c_i$ and a dissolved component with mass fraction c_i. The carrier fluid does not enter the solid phase. The subscript i is dropped from this point on.

For this system the mass transfer term is given by

$$\Gamma = RA(c - c_{\mathrm{eq}}), \tag{8}$$

where R is the reaction rate constant of the soluble component in kg m^{-2} s^{-1} and $A(\mathbf{x}, t)$ is the effective specific surface area (m^2/m^3) available for reaction. c_{eq} is the equilibrium concentration of the soluble component in the fluid, given as a mass fraction. c_{eq} may be a function of position $\mathbf{x}$ and time t, as in the case for varying temperature, pressure, or pH conditions. The specific surface area A is also, in general, a complex function that depends on the porosity ϕ, the distribution of minerals at the pore-grain interface, and whether a mineral is dissolving or depositing.

To simplify (1)–(4), we assume that the density of the fluid and solid phases remains constant. The dispersion/diffusion coefficient $\mathbf{D}$ and the specific surface area A are also approximated as constants, where $\mathbf{D}$ is taken to be equal in all directions. Equations (1)–(4) can now be written as

$$\frac{\partial \phi}{\partial t} = -\Gamma/\rho_s, \tag{9}$$

$$\frac{\partial \phi}{\partial t} + \nabla \cdot (\mathbf{v}\phi) = -\Gamma/\rho_f, \tag{10}$$

$$\phi\frac{\partial c}{\partial t} + \phi \mathbf{v} \cdot \nabla c = D\nabla \cdot (\phi \nabla c) - (1-c)\Gamma/\rho_f, \tag{11}$$

where (11) is a result of subtracting (2) from (4), and (3) need not be considered when the solid is composed of a single soluble component.

Nondimensionalization

In nondimensionalizing equations (5)–(11), we define a characteristic porosity ϕ_0 which controls the characteristic permeability $k_0 = d^2\phi_0^n/b$ and fluid velocity $w_0 = k_0\Delta\rho g/(\phi_0\mu)$ along the z direction. We also define a characteristic lengthscale L and concentration c_0 such that c_0 is the maximum equilibrium concentration in the system. Given these scalings, we define the nondimensional variables, denoted by primed letters:

$$\begin{aligned}
\mathbf{x} &= L\mathbf{x}' \\
\phi &= \phi_0\phi' \\
p &= \Delta\rho g L p' \\
v &= w_0 v' \\
t &= \frac{L}{w_0 c_0}t' \\
c &= c_0 c' \\
c_{\mathrm{eq}} &= c_0 c'_{\mathrm{eq}}(\mathbf{x}, t)
\end{aligned}$$

Two controlling parameters emerge in the problem:

$$Da = \frac{L}{L_{\mathrm{eq}}} \tag{12}$$

$$Pe = \frac{w_0 L}{D}. \tag{13}$$

The Damkhöler number Da defines the ratio between the size of the system L and the chemical equilibration length, $L_{\mathrm{eq}} = (\phi_0 w_0 \rho_f)/(RA)$. The Peclet number Pe defines the ratio between rate of transport by combined diffusion and dispersion to rate of transport by advection.

Using the nondimensional variables and parameters, (5)–(11) can be rewritten as

$$\frac{\partial \phi'}{\partial t'} = -\frac{\rho_f}{\rho_s}\Gamma' \tag{14}$$

$$\nabla \cdot (k'\nabla p') = c_0\frac{\rho_s - \rho_f}{\rho_s}\Gamma' \tag{15}$$

$$c_0\phi'\frac{\partial c'}{\partial t} - k'\nabla p' \cdot \nabla c' = \frac{1}{Pe}\nabla \cdot (\phi'\nabla c') - (1 - c_0 c')\Gamma' \tag{16}$$

$$\Gamma' = \mathrm{Da}(c' - c'_{\mathrm{eq}}(\mathbf{x}, t)) \tag{17}$$

$$k' = \phi'^n \tag{18}$$

Equation (14) describes the temporal evolution of porosity due to reaction. Equation (15) is a Poisson equation for pressure and describes total fluid conservation. Equation (16) states that mineral concentration changes because of reaction, diffusion, and advection. Finally, (17) is used to evaluate the mass transfer rate. This constitutes the basic set of equations for this study. From this point on, primes are dropped with reference to the nondimensional variables.

Basic Properties of the Simulated System

We are particularly interested in a setting that occurs often in geological systems, where there exists a natural continuous gradient in solubility along the main fluid flow path. We show that increasing solubility with height induces overall continuous dissolution, while decreasing solubility with height induces overall precipitation. We also present approximate, one-dimensional, solutions of (14)–(18), in order to gain insight into the behavior of the coupled flow-reaction system.

To simplify the problem we use a linear gradient of solubility in (17) to describe increasing solubility with height, i.e. $c_{\mathrm{eq}}(\mathbf{x}) = z$ where z increases upward. We use $c_{\mathrm{eq}}(\mathbf{x}) = 1 - z$ to describe decreasing solubility. Fluid enters the bottom of the box ($z = 0$) in local equilibrium (i.e., $c(z = 0) = 0$ for increasing solubility with height, and $c(z = 0) = 1$ for decreasing solubility).

When $c_0 << 1$ (an approximation that may be suitable for aqueous systems [*Ortoleva et al.*, 1987] and magmatic systems [*Kelemen et al.*, 1995a; *Aharonov et al.*, 1995]), a first-order quasi-steady state solution to equations (15)–(16) can be obtained: kp_z is approximately constant with height (where p_z is the pressure gradient along the z direction), and mineral concentration in the fluid is

$$c(z) \approx c_{\mathrm{eq}}(z) \pm \alpha(1 - e^{-z/\alpha}). \qquad (19)$$

The plus sign gives the solution for decreasing solubility with height ($c_{\mathrm{eq}}(z) = 1 - z$) and the minus sign gives the solution for increasing solubility with height ($c_{\mathrm{eq}}(z) = z$), and

$$\alpha = k|p_z|/Da \qquad (20)$$

is a measure of fluid disequilibrium. This calculation assumes that diffusion is negligible in the direction parallel to flow, a good assumption outside of the boundary layer, because of the linear nature of the gradient in concentration. Equation (19) predicts that fluid is everywhere out of equilibrium. Therefore from (17), flow through an increasing solubility gradient causes dissolution everywhere with negative mass transfer from rock to fluid. Flow through a decreasing solubility gradient causes precipitation everywhere.

Using (17)–(20), we can rewrite the porosity evolution equation (14) as

$$\frac{\partial \phi}{\partial t} \approx \pm B\phi^n |p_z|(1 - e^{-z/\alpha}), \qquad (21)$$

where $B = \rho_f/\rho_s$. The plus sign applies to a dissolving porous media and the minus sign applies to a precipitating media. The porosity can be easily obtained from (21) if boundary layer effects are neglected.

Constant Pressure Boundary Conditions

Assuming the permeability is constant in space and $c_0 \ll 1$, we obtain from (15), that the pressure gradient p_z is constant throughout the porous matrix. Imposing constant pressure boundary conditions forces p_z to be also constant in time, $p_z = 1$. With these approximations, and neglecting boundary layer effects, (21) becomes $\partial\phi/\partial t \approx B\phi^n$ which has the solution:

$$\phi = \frac{\phi_i}{\left[1 \pm B\phi_i^{n-1}(n-1)t\right]^{1/(n-1)}}, \qquad (22)$$

where $\phi_i = \phi(t = 0)$. Here the minus sign applies for a dissolving porous media, and the plus sign for a precipitating media. Equation (22) predicts that the rate of change of porosity changes with time.

For a dissolving system, porosity increases unstably with time and approaches infinity as $t \rightarrow [B\phi_i^{n-1}(n - 1))]^{-1}$. This unstable growth in porosity is due to the fact that as permeability increases the flux of undersaturated fluid increases, enabling more dissolution and increased flux, in a mechanism similar to the reaction-infiltration instability [*Chadam et al.*, 1986]. During precipitation, in contrast to the dissolution case, the rate of porosity change decreases with time, and $\partial\phi/\partial t \rightarrow 0$ as $t \rightarrow \infty$. This is because the matrix, which is clogging with precipitates, allows less and less flux of nonequilibrated fluid to pass through. Because we imposed constant pressure boundary conditions, flux may freely adjust to changing permeability.

Mineral concentration in the fluid may also change with time. A less obvious result is that (19) and (20) predict that fluid will become increasingly undersaturated with time during dissolution since the permeability k and so α, grow with time. During precipitation the permeability and, as a consequence, α decay with time. Thus fluid supersaturation is reduced with time.

The above predictions are shown in later sections to agree with our simulation results. However, note that (19)-(22) are only applicable when nonlinear effects are small. Solutions are also predicted to break down when $k \rightarrow c_{\mathrm{eq}}Da/|p_z|$ in (19), since the concentration c can not be negative.

Constant Flux Boundary Conditions

If one assumes a constant flux boundary condition, $kp_z = Q$ is constant with both time and height so that Q is also the incoming flux. The porosity (21) then obeys

$$\frac{\partial \phi}{\partial t} \approx \pm BQ(1 - e^{-z/\alpha}), \qquad (23)$$

and, ignoring the boundary layer, porosity changes linearly with time according to:

$$\phi = \phi_i \pm BQt. \qquad (24)$$

Here the plus sign applies for a dissolving porous media, and the minus sign applies for a precipitating media. Equation (24) predicts that the rate of change of porosity is constant with time when the flux of fluid is constant with time. A constant flux boundary condition inhibits the unstable growth of the permeability during dissolution because it restricts the feedback cycle between flux and dissolution. During precipitation, a constant flux boundary condition reduces the permeability faster than when the flux is allowed to adjust itself to the decreasing permeability (compare (22) and (24)).

However, since permeability changes, but flux is forced to remain constant, pressure must adjust at depth. We calculate the excess pressure p_e at any depth $z = 1 - l$ below the surface from Darcy's law. Assuming that pressure is constant at some free surface $p_e(z = 1) = 0$, the nondimensional Darcy's law is given by

$$Q \approx k(\frac{p_e}{l} + 1). \tag{25}$$

Since Q is constant at all times, the excess pressure at depth l is:

$$p_e(l,t) \approx l\frac{k_i - k(t)}{k(t)}, \tag{26}$$

where k_i is the initial permeability at time $t = 0$ and $p_e(l, t = 0)$ is assumed to be zero. $k(t)$ is calculated from (24) and (18) to find an explicit expression for the excess pressure with time and depth:

$$p_e(l,t) \approx l\left(\left[\frac{\phi_i}{\phi_i \pm BQt}\right]^n - 1\right) \tag{27}$$

where plus is for dissolving systems and minus is for precipitating systems. Thus precipitation results in increasing positive excess pressure, which forms because the system clogs itself continuously, while forced to maintain a constant flux via the boundary condition. Of course, permeability will not become negative, and it is probable that if fluid is continuously pumped into the system, fluid pressure at depth will eventually exceed the strength of the rock and cause hydraulic fracturing. The reduction of pressure at depth during dissolution, i.e. formation of a negative excess pressure, is because the same flux occupies an increasing void space.

Description of Numerical Model and Simulation Conditions

Our numerical method for solution of (14)-(18) uses an explicit partial differential equation solver which is implemented on an evenly spaced grid with grid-spacing Δ in each of the respective dimensions and time steps of size Δt. The model allows for flux or pressure specifications at the boundaries.

The solution of the Poisson equation (15) constitutes the step that limits the size of the problem to be solved. Our model uses the iterative multigrid method [*Press et al.*, 1992], an extremely efficient method in which the number of operations only increases linearly with the number of grid points. Operator splitting [*Press et al.*, 1992] is then used to solve (16). The advective contribution is calculated using the "Smolarkiewicz corrected upwind scheme" [*Smolarkiewicz*, 1983], a stable advection scheme, with low numerical diffusion. Low numerical diffusion is achieved by iterative corrections to the calculated flux. The scheme has the standard Courant condition of $\Delta t|\mathbf{Q}_{max}|/\Delta \leq 1/\sqrt{3}$, where $\mathbf{Q} = \phi^{n-1}\nabla p$. The diffusion of concentration in the fluid is calculated using a first-order explicit space-centered scheme [*Press et al.*, 1992].

In the simulations described below, fluid is driven by a pressure gradient from $z = 0$ to $z = 1$, with $p(z = 0) = 1$ and $p(z = 1) = 0$. Our solution for the pressure in the system is equivalent to a background linear pressure gradient (simulating constant buoyancy) with zero excess pressure boundary conditions, $p_e(z = 0, 1) = 0$. We use periodic (wraparound) boundary conditions in the x and y directions. Simulations are performed on a box with 33^3 nodes, varying Da and Pe. We use the permeability exponent $n = 2$, and the maximum concentration is taken as $c_0 = 0.1$. The difference in densities during reaction is neglected in (15) (Boussinesq approximation). The mobile component concentration in the fluid is initially set to equilibrium, $c(z, t = 0) = c_{eq}(z)$. Simulations, except when otherwise specified, are initiated with a randomly noisy porous media, with initial porosity ϕ_i equal to 1 plus a small (1%) Gaussian random white noise. Note that all simulations were performed using the nondimensional equations, and all nondimensional variables have values of order 1.

Simulation Results

Mean System Properties

We present results of four dissolution simulations with $Da = 5, 100$ and $Pe = 10, 200$, and four precipitation simulations with $Da = 10, 100$ and $Pe = 10, 200$. We measure the temporal evolution of some mean properties of our simulated reactive-flow systems and compare them with the simplified theoretical predictions made above. Since we employ constant pressure boundary conditions, we expect unstable growth of permeability and increasing nonequilibrium in the fluid for dissolution, and stably decreasing permeability with fluid approaching equilibrium for precipitation.

The first property we measure is the temporal evolution of the average solute concentration coming out of the box (i.e., $\bar{c}(z = 1)$). Results from dissolution simulations are shown in Figure 1a and compared with the scaling arguments given by (19), where we use the predicted permeability from (22) and (18), with $p_z = 1$, to calculate α at any given time. Dissolution produces increasing deviation from equilibrium with time and fits the scaling arguments of the previous section at small times. Nonlinearity probably influences behavior at $t \gg 0$. For $Da = 5$, deviation from equilibrium flattens out because of the growth of the boundary layer with time as the permeability increases. Reducing the Pe from $Pe = 200$ to 10 produced identical simulation results. The evolution of the concentration of fluid coming out of the box in the case of flow coupled with precipitation is shown in Figure 1b. In this case, fluid approaches equilibrium, and nonlinear effects are expected to be small (no unstable growth). Note the different vertical scales in Figures 1a and b.

We next study the evolution of the average permeability during coupled flow and reaction. Average permeability is measured in simulations by taking the spatial average (over the x and y directions) of permeability only at $z = 1$ to avoid including boundary layer effects. Simulation results are shown in Figure 2. Scaling arguments (equations

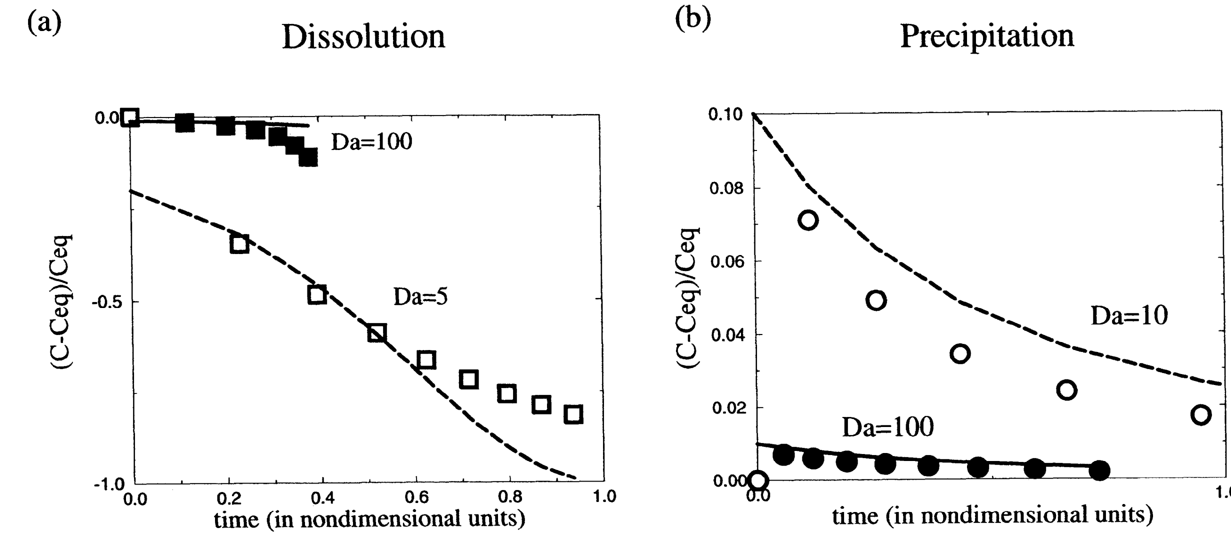

Figure 1. Average deviation from local equilibrium of mineral concentration in the liquid coming out of the top the box, $(c - c_{eq})/c_{eq}$, as a function of time. (a) Results from dissolution simulations: $Da = 100$ in solid squares and $Da = 5$ in open squares. (b) Results from precipitation simulations: $Da = 100$ in solid circles and $Da = 10$ in open circles. Lines are predictions from linear analysis (equations (18)- (22)). The dissolution simulation performed at $Da = 100$ ends after a relatively short time, since the channeling instability produces increasingly sharp spatial gradients in permeability between channels and low-permeability walls to the point where our numerical scheme becomes unstable. Theory and simulations do not agree at $t = 0$ because the initial conditions of the simulations are not the theoretical quasi-steady solutions.

(18) and (22)) predict that rates of permeability change are independent of Da. During precipitation simulations, permeability reduction is, indeed, found to be independent of Da number. During dissolution, simulations performed with $Da = 5$ show a good agreement with linear theory at early times. However, as permeability increases with time, boundary layer effects become important. Since boundary layer effects were neglected in obtaining the porosity in (22), one expects a deviation from the approximate solutions when they become important. Simulations performed with $Da = 100$ show a more rapid growth of permeability than predicted by linear analysis, probably because of coupled nonlinear effects which become increasingly important as disequilibrium and hence mass transfer terms grow during dissolution.

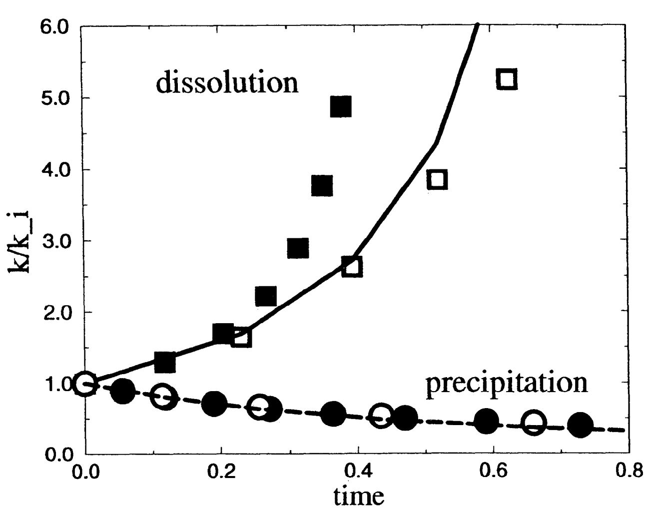

Figure 2. Temporal evolution of the permeability k/k_i (where k_i is the initial permeability), measured at the top of box for dissolution (in squares) and precipitation (in circles) simulations. Solid symbols indicate results from simulations with $Da = 100$. Open symbols indicate results from simulations with $Da = 10$. Solid (dashed) line is linear prediction for permeability evolution during dissolution (precipitation) from equations (18) and (22).

Evolution of Statistical Properties During Flow and Reaction

In this section we investigate the temporal evolution of the statistical properties and morphology of porous media due to flow and reaction. To quantify our results we measure the autocorrelation functions of porosity and flux $C(\mathbf{r})$. The autocorrelation function measures the correlation between a scalar property Φ (e.g., the porosity) at position vectors $\mathbf{r}'$ and $\mathbf{r}' + \mathbf{r}$ (i.e., the likelihood that two positions separated by a lag $\mathbf{r}$ have the same value of Φ)

$$C(\mathbf{r}) = 1/V \int_V \Phi(\mathbf{r}' + \mathbf{r})\, \Phi(\mathbf{r}')\, d\mathbf{r}', \tag{28}$$

where V is the sample volume. The autocorrelation function is obtained using the Wiener-Khinchin theorem [e.g., *Bracewell*, 1978]. Practically, this is done by taking the inverse Fourier transform of the 3-D power spectra of Φ. $C(\mathbf{r})$ is then normalized to 1 and ranges between -1 and 1. An increase in the value of the correlation function along the flow direction with time indicates that high (low) porosity regions are preferentially found up or downstream to other high (low) porosity regions. Thus the correlation function can be viewed as a measure of channeling. A decrease in the value of $C(\mathbf{r})$ indicates destruction of correlated paths.

The second statistical measure we use is the evolution of histograms of flux and porosity, where the width of distributions indicates the variability to be found in the media. For example, a narrowing distribution of flux indicates that flow is becoming increasingly uniform and homogeneous.

Dissolution. Figure 3a shows an isosurface of the flux at $t = 0.4$ from a simulation with $Da = 100$ and $Pe = 200$. The isosurface reveals that fingers of high porosity have evolved from the initially randomly constructed porous media. This channeling instability [*Aharonov et al.*, 1995] is similar to the reactive infiltration instability [*Chadam et al.*, 1986; *Steefel and Lasaga*, 1990]. Channels grow because regions where the permeability is initially slightly higher than average (because of the 1% noise in the initial porosity distribution) allow increased flow of undersaturated material from below and so experience relatively more dissolution then neighboring lower-permeability regions. Thus high-permeability regions dissolve more rapidly, increasing their permeability even more, in a positive feedback mechanism.

Figure 4 shows the evolution of the porosity and flux histograms for the same simulation ($Da = 100$ and $Pe = 200$). The mean value of the variables at the time when histograms were calculated has been subtracted to enable comparison of results at different times. During dissolution the histograms widen with time. This increased variance reflects a growing instability in the porous media. The fact that flux shows a larger variability than porosity can be attributed to two effects: (1) flux amplifies variations in porosity for a porosity-permeability relationship such as (7) with exponent $n > 1$ and (2) the contrasting fast and slow regions of flow may reflect the efficient spatial organization of porosity. The spatial rearrangements can be observed in Figure 4c as an increase in the autocorrelation function of the porosity in the direction parallel to the flow (lag in z), which means that high porosity is likely to be found below or above other regions of high porosity while low-porosity regions will be found adjacent to other low-porosity regions (i.e., there are elongated pipes of high permeability). The increase in correlations is most prominent along the flow direction, while there is nearly no change in the correlation function perpendicular to the flow direction.

We investigated the effect of changing the Da and Pe numbers on the channeling instability by looking at the changing value of the porosity autocorrelation function along the direction of flow at a particular chosen lag of $1/6$ of the box. The rate of increase of the correlation function indicates the rate of organization of the matrix into channels. The lag at which the correlation function was measured was chosen to be smaller than the box size but larger than a few nodes and could just as well have been 1/3 or 1/4 of the box. Figure 5 shows the unstable growth of correlations along the flow path for $Da = 100$. The effect of increasing diffusion rates ($Pe = 10$) slows the onset of the instability somewhat but does not inhibit its growth. When Da is lowered from 100

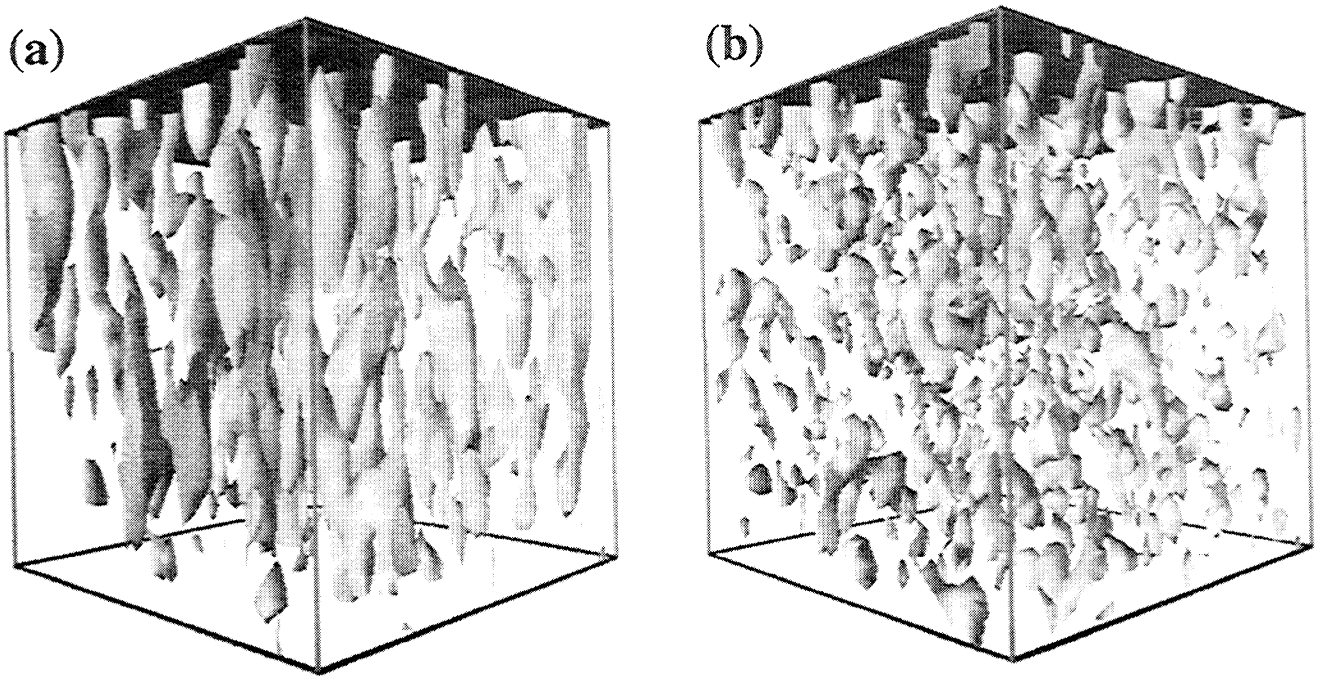

Figure 3. Three dimensional isosurfaces of the flux at $t = 0.4$, obtained in (a) dissolving and (b) precipitating porous media. Main flow direction is upward. Figure 3a shows an isosurface of flux in a porous media which has undergone dissolution. The isosurface has a value of 4.95 $w_0\phi_0$, and the range of flux values at this time is between 3.25 and 6.19. The isosurface shows formation of elongated permeability structures parallel to flow direction. Figure 3b shows an isosurface of flux in a porous media which has undergone precipitation. The isosurface has a value of 0.815 $w_0\phi_0$, where the flux range at this time is 0.695 − 0.872. The isosurface shows diffuse and uniform structures and the complete disappearance of the channelized structures that were present at the beginning of the simulation.

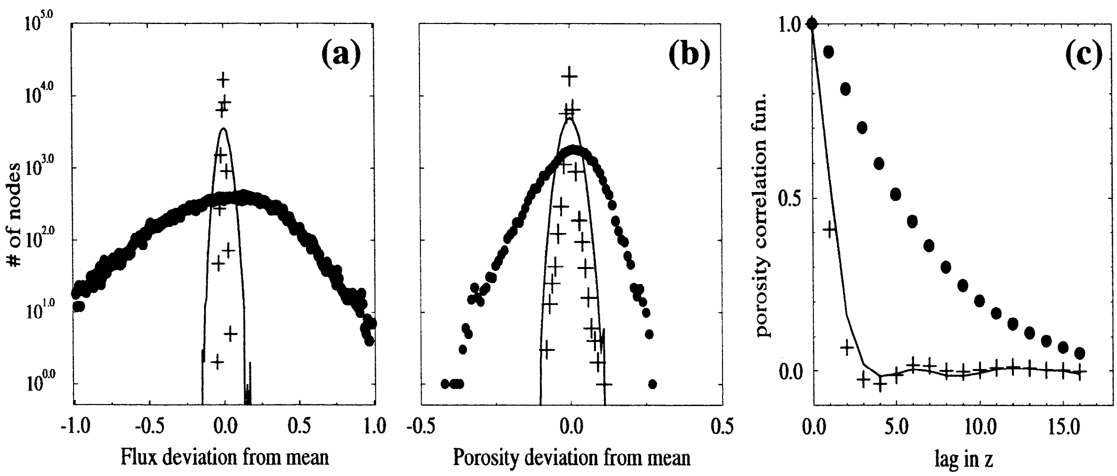

Figure 4. Histograms of flux and porosity, and correlation functions of porosity in a dissolving and precipitating porous media. The mean value of the variables at any time step was subtracted when constructing the histograms to enable comparison of results from different times. Bin size is constant. The correlation functions of porosity shown are for lags along the flow direction. Initial random configurations for dissolution simulations are in solid lines. Results after dissolution are in circles, and results after precipitation are indicated by pluses (in precipitation we used the dissolved media as the initial configuration). (a) The variability in flux after dissolution (circles) has increased considerably compared to the narrow initial variability (solid line), as is expected in unstable growing channels with regions of fast and slow flow. Precipitation acting on the channelized media has a homogenizing effect that results in a spiky histogram (in pluses). (b) The change in porosity variability is smaller but has the same qualitative characteristics as Figure 4a. (c) Porosity autocorrelation function in the direction parallel to flow is considerably enhanced after dissolution, compared to the initial random media, consistent with elongated channel formation. Precipitation, acting on the correlated porous media originally formed by dissolution, has destroyed the correlations parallel to the flow direction.

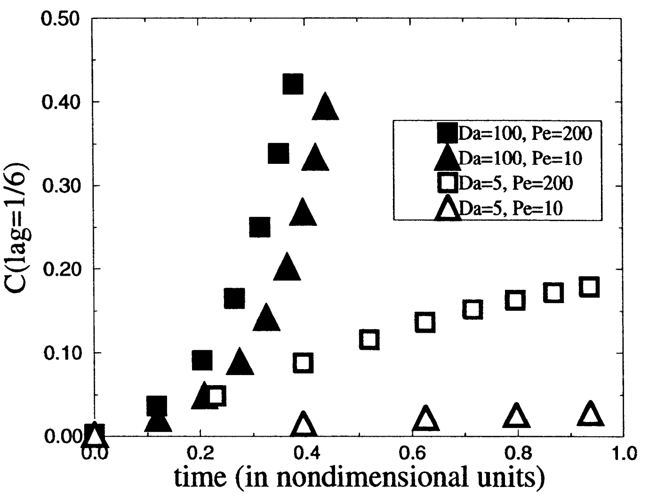

Figure 5. Porosity correlation function along the flow direction, at a given lag of $1/6$, as a function of nondimensional time. The along-flow porosity correlation function is indicative of the organization of porosity into high- and low-porosity channels along the flow direction. Simulation results for $Da = 100$ show that the correlation function grows in an unstable manner, both for $Pe = 200$ (solid squares) and $Pe = 10$ (solid triangles). Simulation with $Da = 5$ and $Pe = 200$ (open squares) shows some increase in the correlation function but not unstable growth of channels. Simulations with $Da = 5$ and $Pe = 10$ (open triangles) do not show increase in the porosity correlation function and therefore indicate uniform, rather than channelized, dissolution.

to 5, the correlation function does not approach unity, that is channels do not grow as efficiently.

Precipitation. To contrast the effect of dissolution and precipitation, we initiated a precipitation simulation with $Da = 100$ and $Pe = 200$, but instead of a random porosity we initiated the simulation using the dissolved, channelized porous matrix formed by the dissolution experiment with $Da = 100$ and $Pe = 200$. Figure 3b shows an isosurface of the flux at $t = 0.4$. The isosurface reveals that the initial channels of high permeability have been destroyed, and instead flow is uniform. During the course of our simulations we have observed that most precipitation occurs close to the entrance to preferred paths for flow, and as the entrance clogs up, flow is diverted to other paths. This mechanism causes flow to become diffuse and uniform, as observed in the narrowing flux and porosity histograms in Figure 4a and b. Since flux and precipitation are diverted from high-permeability paths once some low permeability barrier forms at the entrance, precipitation preferentially causes low permeability regions to form adjacent to high permeability regions, resulting in a negative change in the correlation function. In other words, reduction in the correlation function implies a reduction of connectivity in the matrix. The histograms also reveal that precipitation acts to smooth the initial variability in flux and porosity, thus bringing the distributions close to the original statistical state that existed before dissolution has operated. The correlation function of the porosity, shown in Figure 4c, demonstrates that correlations along the direction parallel to flow are reduced and, indeed, nearly overlap the initial random correlations that existed before the dissolution simulation.

We investigated the effect of changing the Da and Pe numbers on the precipitation dynamics by simulating precipitation in an initially random porous media and looking at the changing value of the porosity autocorrelation function along the direction of flow at a particular chosen lag of $1/6$ of the box, exactly as was done for dissolution. Figure 6 shows the reduction in the value of the autocorrelation function and the formation of weak, but noticeable, negative correlations along the flow path for all parameter ranges.

Transition from dissolution to precipitation. We are next interested to know what happens when fluid flows from an area where it can dissolve the porous matrix to an area where it is precipitating. Such a transition is expected to occur along the ascent paths of melt in the mantle, as well as fluid paths across isotherms in sedimentary basins. To simulate a transition between the dissolution to precipitation, we impose an equilibrium saturation that first increases and then decreases with height by using $c_{eq} = \sin(\pi z)$. This allows for dissolution to occur to up to half the box length and then for crystallization to occur in the second half. Fluid is initially in equilibrium with respect to the mobile component. Fluid continuously enters the box in equilibrium (i.e., $c(z = 0) = 0$), and the simulation is performed with $Da = 100$ and $Pe = 200$.

We observe, as expected, that channels form in the dissolving region but not in the precipitating region. Figure 7a shows average porosity (over x and y) as a function of height at $t = 0.5$. Porosity increases from its initial value (because of dissolution) up to half the box, after which a decrease in porosity occurs (because of precipitation). Figure 7b shows excess pressure as a function of z, also at $t = 0.5$. A growing overpressure occurs close to the transition from dissolution to precipitation. In this rigid matrix the difference in porosity between the dissolving and the crystallizing regions and the overpressure associated with the transition continue to increase with time.

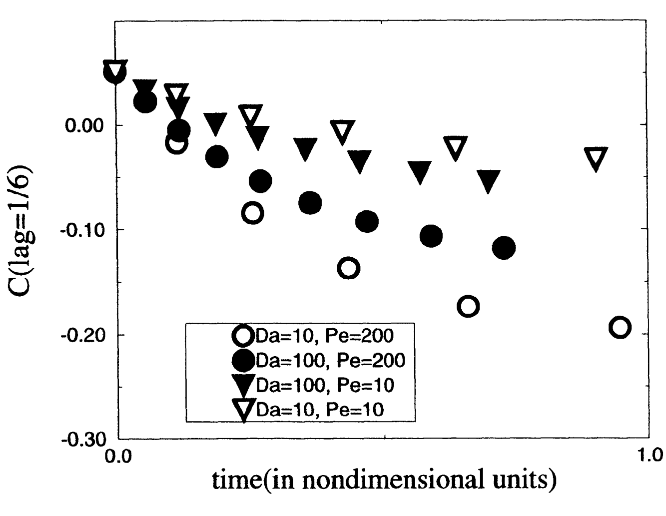

Figure 6. Porosity correlation function along the flow direction, at a given lag of $1/6$, as a function of nondimensional time. The initial porous media was randomly constructed, and it is seen that precipitation results in formation of slightly negative correlations along the flow path. This is due to the increased precipitation in the most permeable areas, after which the flow is diverted, leaving high-permeability regions adjacent to low-permeability regions.

Discussion

We have presented a 3-D reactive-flow model, some theoretical predictions, and results from simulations contrasting dissolution and precipitation effects at different Da and Pe numbers. In the simulations, we have used constant pressure boundary conditions which allow the system to adjust naturally to feedbacks that control the flux. We find that under such conditions permeability and undersaturation grow unstably during dissolution. During precipitation, permeability and supersaturation decrease at a rate which decreases with time. Our approximate calculations suggest that the evolution of the system depends on boundary conditions. For example, constant flux, instead of constant pressure, boundary conditions produce increasing deviations of pressure at depth. For both boundary conditions, however, scaling arguments for the mean evolution of porosity, (22)-(24), predict that outside of a boundary layer of thickness $1/Da$, porosity changes at a rate that is independent of Da number.

The control parameters in a coupled flow and reaction system are the Da and Pe numbers. These parameters depend on the modeled system size. Behaviors observed at high Da or Pe numbers will also appear in systems with low reaction rates or high diffusivities, provided that the system size L is large enough. The intrinsic length scales in the problem are the equilibration length L_{eq} and the diffusion length scale D/w_0. One expects that, in a rigid matrix, reaction features such as spacing of channels and boundary layer thickness will scale with those intrinsic length scales. The choice of c_0 mainly controls the timescales of growth of features in such reactive systems but otherwise does not change the qualitative behavior of the system.

Dissolution

We find that in three dimensions, with a gradient in solubility in a rigid matrix, dissolution channels form when $Da \gg 1$. The channels are elongated in the direction parallel to flow, span the whole upwelling-dissolving region (as predicted theoretically in two dimensions [*Aharonov et al.*, 1995]), and have a pipe-like structure in 3-D. The morphology of the channels is not completely understood in 3-D.

Statistical analysis has shown that when Da is high, porosity correlations increase continuously in the direction parallel to the main flow direction indicating channel growth with no limiting vertical length scale. The porous matrix has thus become anisotropic: correlated and channelized along the flow direction, but with only minor increases in correlations in the direction perpendicular to the main flow direction.

Decreasing the Da number increases the width of the boundary layer, in which channels do not grow efficiently (a

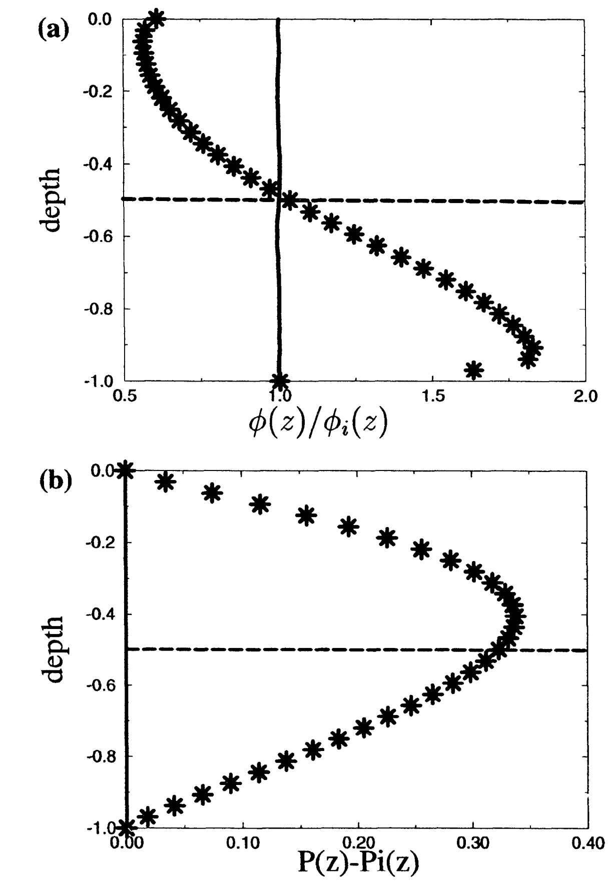

Figure 7. Porosity and pressure profiles (averaged over x and y) as a function of depth, obtained from simulations where fluid flows from an area of dissolution to an area of precipitation. Simulations are performed with constant pressure boundary conditions. The onset of precipitation, at depth $= -1/2$, is marked by a dashed line. (a) The initial porosity $\phi_i(z) \sim$ const (solid line). At a later time ($t = 0.5$, stars), porosity $\phi(z)$ has increased in the dissolving region (depth $< -1/2$) and decreased in the precipitating region (depth $> -1/2$). (b) The initial pressure $P_i(z)$ increased linearly with depth. After flow and reaction ($t = 0.5$, in stars) the pressure distribution $P(z)$ has changed. $P(z) - P_i(z)$, the deviation from the initial linear ramp, shows a pronounced maximum close to the depth at which the transition from dissolution to precipitation occurs. This overpressure is dynamic and forms because of the evolving permeability structure.

similar result has been noted for dissolution fronts by *Daccord and Lenormand* [1987] and *Hoefner and Fogler* [1988], where decreasing Da produced a wide reaction zone and no channeling). Systems of size $L \gg L_{eq}$ may exhibit unstable channel growth such as we have observed for high Da numbers, since in such systems boundary layer thickness is small relative to system size. For systems with slow reactions, one may recapture results for high Da number systems by simply "zooming out" and considering a larger system.

In a result similar to those for dissolution fronts [*Ortoleva et al.*, 1987], we find that reducing the Pe number does not change the nature of the instability but increases the width of the channels and the spacing between them and lowers their growth rate. We predict that channels may be observed in systems with size L much larger than the diffusion length scale. It is interesting to note that we have not yet been able to determine whether there exists a prefered horizontal wavelength for channel growth or whether channels grow on available heterogeneities greater than the diffusion length scale. Nevertheless, independent of their width, the vertical extent of the channels spans the whole region over which dissolution occurs.

Precipitation

Regions of high permeability allow higher flux of nonequilibrated fluid from downstream and, as a consequence, more reaction. In a supersaturated fluid the result is increased clogging in the high-permeability paths, a stabilizing effect that will reduce initial variability in permeability. We have contrasted precipitation with dissolution by using a dissolved, channelized porous matrix as the initial configuration upon which flow coupled with precipitation operated. Simulations show that precipitation efficiently reduces, and eventually destroys, any existing correlations in the direction parallel to the flow. In precipitation, as in dissolution, the porous matrix becomes increasingly anisotropic, but here alternating patchy regions of low and high permeability form along the main flow direction. This in effect reduces the connectivity of the porous matrix. Although the permeability structure appears to be rough and unorganized, as seen in Figure 3b, the porous media is actually undergoing a self-organization to produce increasingly uniform flow fields, as seen in Figure 4a and 4b. We do not find any significant differences in results for a variety of Da and Pe numbers.

Transition Zones Between Dissolution and Precipitation

A transition zone between dissolution and crystallization is shown by our simulations to produce a monotonically increasing overpressure above the initial pressure in the system. The transition zone, which is marked by a reaction boundary layer, is expected to be relatively localized when the system under consideration has a lateral extent L larger than L_{eq}.

The calculated overpressure has a dynamic source [*Neuzil*, 1995] and would not occur if the fluid were stationary. The decreasing permeability in the crystallizing region acts as a roadblock to the increasing flux from the dissolving region. This effect can be qualitatively understood from the first-order calculation of pressure under constant flux boundary conditions given in (26). Such an overpressure will only grow until it exceeds the strength of the porous matrix, after which a fracture will form through which fluid may flow and relieve the overpressure. The effect is expected to be somewhat damped by the addition of compaction and decompaction and is a subject of future study.

Implications for Geological Systems

Understanding reactive flow through porous media may shed some light on various rock-fluid systems. We have chosen to concentrate on two widely different systems: the first is melt extraction from the mantle, and the second is formation of overpressurized zones in sedimentary basins.

It should be mentioned that although in our equations dissolution and precipitation differ only by sign and appear to be reversible processes, the field manifestation is much more complex. Reactions usually involve more than just a single mineral and fluid. In many systems, dissolution and precipitation may not be completely symmetrical, and certainly the physical effects of these processes will be a function of the porous media on which the processes operate. For example, dissolution channels enhance preexisting heterogeneities in the porous matrix. The initial extent and distribution of heterogeneities (pores and fractures) may influence the organization and growth of channels.

In order to obtain realistic temporal and spatial descriptions of permeability, one would desire a better description of the porosity-permeability relation. This function is strongly influenced by microscale distribution of precipitates [*Aharonov et al.*, 1997]. For example, clay precipitates may induce an immobile fluid layer at the pore-grain boundary, with an effective reduction in permeability which is many orders of magnitude greater than that obtained by merely considering the clay mass precipitated. Such effects need to be included before quantitative predictions can be made, especially in precipitating systems, although the qualitative behavior of the system should not be greatly affected.

Compaction of solid phase also needs to be considered when modeling natural systems. Nevertheless, even in the presence of compaction, dissolution is expected to produce unstable growth of channels [*Aharonov et al.*, 1995; *Spiegelman et al.*, 1996].

Melt Extraction from the Mantle

Our simulations support the recent proposition [*Kelemen et al.*, 1995a] that modes of melt extraction from the mantle, as well as melt chemistry, may be, in part, controlled by whether melts partially dissolve their surroundings or partially crystallize during upwelling. The Earth's mantle ascends adiabatically below mid-ocean ridges, producing partial melting in decompressing peridotite. If it were transported in a chemically closed system, liquid created at a given depth and rising would remain undersaturated in pyroxene for most of its ascent path. In an open system, reaction between ascending liquid and peridotite will incongruently dissolve pyroxene, with a net increase in the liquid mass [*Sleep*, 1975; *Kelemen*, 1990; *Kelemen et al.*, 1995a]. Our simulations of increasing fluid mass with height show that elongated high-permeability channels form during reactive porous flow in three dimensions when the system size is much larger than the chemical equilibration length L_{eq}. For a more extensive discussion of why our simulation conditions may represent upwelling beneath mid-ocean ridges see *Kelemen et al.* [1995a] and *Aharonov et al.* [1995]. The vertical channels span the whole region of melting in a rigid matrix. These results are qualitatively similar to the 2-D linear predictions [*Aharonov et al.*, 1995] obtained for a compacting-dissolving matrix. Parameter ranges for reactive melt flow in the mantle are not well constrained, but Da numbers will be high, with correspondingly short equilibration lengths; L_{eq} is likely to be less than about 10 m. Pe numbers for melt flow in the mantle are also likely to be high, of the order of 10^3 to 10^6 over a distance of 100 m. Further discussion of relevant parameter ranges for melt flow in the mantle are given by *Aharonov et al.* [1995].

As detailed by *Kelemen et al.* [1995a, 1995b], the formation of such channels may explain the observation of chemical disequilibrium between mid-ocean ridge basalt and surrounding depleted peridotite [*Johnson et al.*, 1990; *Johnson and Dick*, 1992]. Some kind of channels have been inferred in order to explain the geochemical observations [*Spiegelman and Kenyon*, 1992; *Hart*, 1993], but the formation mechanism for channels in the viscously deformable parts of the mantle was unclear. Recent work [*Kelemen et al.*, 1995b] suggests that many replacive dunites found in ophiolites are dissolution channels that formed in the upwelling mantle beneath oceanic spreading ridges. These are elongated bodies in 2-D outcrops, with lengths from 10 to 10^4 m or more, and length/width ratio > 10. For more discussion on the size and distribution of channels, see *Kelemen et al.* [1997b] and references therein.

When melts from the adiabatically upwelling mantle enter the overlying, conductively cooled "lithosphere" or "tectosphere," , the melts will begin to cool. Beneath mid-ocean ridges, the conductively cooled region is relatively thin. In contrast, beneath hot spot volcanos, ascending melts must pass through a thick tectosphere. As noted by *Kelemen* [1986, 1990] and *Kelemen et al.* [1993, 1995a], thermal models of subduction zones suggest that melt initially heats and then cools as it ascends through the mantle wedge. Our simulations have shown that when liquids crystallize following a decreasing gradient in solubility, the flow becomes diffuse and homogeneous, even where channels of focused flow were initially present. This result is in agreement with inferences based on the chemistry of lavas and mantle samples from hot spots and subduction-related arcs [see *Kelemen et al.*, 1993, 1995a, and references therein], which show the effects of mantle/magma interaction at lower melt/rock ratios compared to mid-ocean ridge basalts

A transition zone between dissolution and crystallization occurs near the base of the conductively cooled lithosphere. Where this transition occurs depends to some extent on the importance of advective heat transfer due to melt migration, which is not explicitly included in our model. However, calculations of the thermal Peclet number for porous flow indicate that advective heat transfer will not distort a regional, steady state geotherm until all the flux is in channels which occupy $\ll 0.1\%$ of the solid volume. (e.g., J. Korenaga and P. Kelemen, paper in preparation, 1997).

The transition from dissolution to crystallization will occur, at some depth, in any scenario. Such a transition is shown by our simulations to have monotonically increasing porosity and overpressure over time. We speculate that melt will pond in sills within the transition zone, and then increasing overpressure may lead to hydrofracturing of the rock, which in turn relieves some of the pressure [*Kelemen* *et al.*, 1997a]. After some period of melt extraction, precipitation will occur within these fractures. Our simulations show that crystallization will be more rapid in the fractures than in the surrounding porous matrix, since the fractures are initially the highest-permeability channels for flow. The fractures may heal, with the cycle repeating itself indefinitely. This scenario is consistent with the presence of dikes, fractures filled with the products of crystal fractionation because of cooling of magma, formed away from spreading ridges and found in ophiolite mantle sections. In contrast, evidence for melt-filled fractures is not found in features formed in the adiabatically upwelling region beneath mid-ocean ridges axes [e.g., *Kelemen et al.*, 1997b]. More work is needed to theoretically evaluate the likelihood of this process in viscously compacting porous media and to investigate geological evidence for hydrofractures originating at the base of the tectosphere.

Precipitation and Formation of Abnormal Pressure Zones in Sedimentary Basins

A common feature found in sedimentary basins, especially in rapidly compacting ones, is abnormally high pressure zones. These often cut across geological structures, and follow thermoclines [*Hunt*, 1990]. It is thus possible that some (but by no means all) of these high-pressure zones are associated with the onset of precipitation of certain pore-lining minerals (e.g., carbonates or clays) during upward flow of fluids. This hypothesis is especially appealing because of the fact that many high-pressure zones are found close to the same depth (around 3000m) [*Hunt*, 1990], strongly suggesting an underlying temperature or pressure dependent reaction involving precipitation of a common mineral.

Our simulations results, in which we find reduction of connectivity and preferential clogging of fast flow paths during precipitation, suggest that precipitation coupled with flow may cause reduction in permeability at a relative rate which is faster than the rate of reduction in porosity ($\dot{k}/k > \dot{\phi}$). When $\dot{k}/k > \dot{\phi}$ pore pressure will increase with time, simply because pore fluids become trapped [*Nur and Walder*, 1990]. As well as this static increase in pressure, a dynamic [*Neuzil*, 1995] increase in pore pressure (i.e., excess pressure that exists only in connection with flow) is expected at the depth of the onset of precipitation, similarly to our simulation for the transition from dissolution to precipitation (i.e., a "roadblock" effect).

If flow coupled with precipitation is, indeed, the mechanism responsible for formation of some of these high-pressure zones, high-pressure zones will be found in rapidly sedimenting and compacting basins (where fluid flow effects may be important), with the seal depth remaining constant even as sediments continue to subside. It is interesting that crystallized fractures are often found above high-pressure zones, and within the seals, but not below them, suggesting periodic fracturing similar to the mechanism proposed for magma transport from the the base of the tectosphere. Such fractures are found to reseal relatively rapidly, while the high-pressure zone maintains some of its overpressure during this cycle (observations are based on findings of the Federal Power Commission (1973), as detailed by *Hunt* [1990]). Hydraulic pulses and formation of high pressure zones have been studied before [e.g., *Nur and Walder*, 1992; *Dewers and Ortoleva*, 1994], but here the combined dynamic and static source of the overpressure which arise naturally from flow and precipitation point to a localized and specific sealing mechanism. Furthermore, preferential precipitation in the fastest flow paths may help explain why seals maintain their overpressure over time and why hydrofractures seal rapidly. On the basis of equilibration lengths estimated by *Knapp* [1989], sedimentary basins have L_{eq} smaller than a few tens of meters, which suggests that high Da number regimes are appropriate for describing sedimentary systems larger than a few hundreds of meters. Further work is underway to investigate the effects of compaction and elasticity.

Acknowledgments. This work was supported by NSF grants OCE93-14013 and OCE95-30307. We wish to thank J. Fredrich, H. Stockman and another anonymous reviewer for their excellent comments and thorough review. E.A. wishes to thank D. Rothman, J. Olson, and E. Tenthorey for helpful discussions.

References

Aharonov, E., J. Whitehead, P. B. Kelemen, and M. Spiegelman, Channeling instability of upwelling melt in the mantle, *J. Geophys. Res.*, *100*, 20,433–20,450, 1995.

Aharonov, E., A. Thompson, and D. H. Rothman, Sedimentary rocks: Transport properties and diagenesis linked by microscale geometry, *Geology*, *In press*, 1997.

Bear, J., *Dynamics of Fluids in Porous Media*. Dover, Mineola, New York, 1972.

Bekri, S., F. Thovert, and P. Adler, Dissolution in porous media, *Chem. Eng. Sci.*, *49*, 1–27, 1995.

Bodinier, J. L., Geochemistry and petrogenesis of the Lanzo peridotitie body, *Tectonophysics*, *149*, 67–88, 1988.

Boudier, F., and A. Nicolas, Structural controls on partial melting in the Lanzo peridotites, in *Magma Genesis*, edited by H. B. Dick, pp. 63–78, Portland. Oreg. Dep. of Geol. and Miner. Ind., 1977.

Bracewell, R., *The Fourier Transform and Its Applications*. McGraw-Hill, New York, 1978.

Chadam, J., D. Hoff, E. Merino, P. Ortoleva, and A. Sen, Reactive infiltration instability, *IMA J. Appl. Math.*, *36*, 207–221, 1986.

Daccord, G., and R. Lenormand, Fractal patterns from chemical dissolution, *Nature*, *325*, 431–432, 1987.

Dewers, T., and P. Ortoleva, Nonlinear dynamical aspects of deep basin hydrology: fluid compartment formation and episodic fluid release, *Am. J. Sci.*, *294*, 713–755, 1994.

Dick, H., Evidence of partial melting in the Josephine peridotite, in *Magma Genesis*, edited by H. B. Dick, pp. 63–78, Portland. Oreg. Dep. of Geol. and Miner. Ind., 1977.

Hart, S. R., Equilibration during mantle melting: A fractal tree model, *Proc. Natl. Acad. Sci. U.S.A.*, *90*, 11,914–11,918, 1993.

Hoefner, M., and H. Fogler, Pore evolution and channel formation during flow and reaction in porous media, *AIChE J.*, *34*, 45–54, 1988.

Hunt, J. M., Generation and migration of petroleum from abnormally pressured fluid compartments, *Amer. Assoc. Petrol. Geol. Bull.*, *74*, 1–12, 1990.

Johnson, K., and H. Dick, Open system melting and the temporal and spatial variation of peridotite and basalt compositions at the Atlantis II fracture zone, *J. Geophys. Res.*, *97*, 9219–9241, 1992.

Johnson, K., H. Dick, and N. Shimizu, Melting in the oceanic upper mantle: An ion microprobe study, *J. Geophys. Res.*, *95*, 2661–2678, 1990.

Kelemen, P., Assimilation of ultramafic rock in subduction related magmatic arcs, *J. Geol.*, *94*, 829–843, 1986.

Kelemen, P., Reaction between ultramafic wall rock and fractionating basaltic magma, *J. Petrol.*, *31*, 51–98, 1990.

Kelemen, P., H. Dick, and J. Quick, Production of harzburgite by pervasive melt rock-reaction in the upper mantle, *Nature*, *358*, 635–641, 1992.

Kelemen, P., N. Shimizu, and T. Dunn, Relative depletion of niobium in some arc magmas and the continental crust, *Earth Planet. Sci. Lett.*, *120*, 111–134, 1993.

Kelemen, P., J. Whitehead, E. Aharonov, and K. Jordahl, Experiments on flow focusing in soluble porous media with applications to melt extraction from the mantle, *J. Geophys. Res.*, *100*, 475–496, 1995a.

Kelemen, P. B., N. Shimizu, and V. J. Salters, Extraction of MORB from the upwelling mantle by focused flow of melt in dunite channels, *Nature*, *375*, 747–753, 1995b.

Kelemen, P. B., K. Koga, and N. Shimizu, Geochemistry of gabbro sills in the crust-mantle transition zone of the Oman ophiolite: implications for the origin of the oceanic lower crust, *Earth Planet. Sci. Letts.*, *146*(3–4), 475–488, 1997a.

Kelemen, P. B., G. Hirth, N. Shimizu, M. Spiegelman, and H. J. B. Dick, A review of melt migration processes in the adiabatically upwelling mantle beneath oceanic spreading ridges, *Phil. Trans. R. Soc. London A*, *355*(1723), 283–318, 1997b.

Knapp, R. B., Spatial and temporal scales of local equilibrium in dynamic fluid-rock systems, *Geochim. Cosmochim. Acta*, *53*, 1955–1964, 1989.

Neuzil, C. E., Abnormal pressures as hydrodynamic phenomena, *Am. J. Sci.*, *295*, 742–786, 1995.

Nur, A., and J. Walder, Time-dependent hydraulics in the Earth's crust, in *The Role of Fluids in Crustal Processes*, edited by E. Comm. on Geosci., and Resour., pp. 113–127. Natl. Sci. Found., Arlington, VA, 1990.

Nur, A., and J. Walder, Hydraulic pulses in the Earth's crust., in *Fault Mechanics and Transport Properties of Rocks*, edited by B. Evans, and T. F. Wong, pp. 461–473. Academic, San Deigo, Calif., 1992.

Ortoleva, P., J. Chadam, E. Merino, and A. Sen, Geochemical self-organization II: The reactive-infiltration instability, *Am. J. Sci.*, *287*, 1008–1040, 1987.

Ozawa, K., Melting and melt segeregation in the mantle wedge above a subduction zone: Evidence from the chromite-bearing periodotites of the miyamori ophiolite complex, *J. Petrol.*, *35*, 647–678, 1994.

Phillips, O. M., *Flow and Reactions in Permeable Rocks*. Cambridge Univ. Press, New York, 1991.

Press, W., S. Teukolsky, W. Vetterling, and B. Flannery, *Numerical Recipes in FORTRAN*. Cambridge Univ. Press, New York, 2nd edn., 1992.

Quick, J., The origin and significance of large, tabular dunite bodies in the Trinity peridotite, northern California, *Contrib. Mineral. Petrol.*, *78*, 413–422, 1981.

Richardson, S., and H. McSween, *Geochemistry, Pathways and Processes*. Prentice-Hall, Englewood Cliffs, N. J., 1989.

Sleep, N., Formation of oceanic crust: Some thermal constraints, *J. Geophys. Res.*, *80*, 4037–4042, 1975.

Smolarkiewicz, P., A simple positive definite advection scheme with small implicit diffusion, *Mon. Weather Rev.*, *111*, 479–486, 1983.

Spiegelman, M., Flow in deformable porous media, 1, Simple analysis, *J. Fluid Mech.*, *247*, 39–63, 1993.

Spiegelman, M., and P. Kenyon, The requirements for chemical disequilibrium during magma migration, *Earth. Planet. Sci. Lett.*, *109*, 611–620, 1992.

Spiegelman, M., E. Aharonov, and P. B. Kelemen, The compaction reaction: Magma channel formation by reactive flow in deformable media (abstract), *EOS Trans. AGU*, *77*(46), F783, Fall Meet. Suppl., 1996.

Steefel, C., and A. Lasaga, Evolution of dissolution patterns, in *Chemical Modeling in Aqueous Systems II*, edited by D. Melchior, and R. Bassett, pp. 212–225. Am. Chem. Soc., Washington, D.C., 1990.

Steefel, C. I., and A. C. Lasaga, A coupled model for transport of multiple chemical species and kinetic precipitation/dissolution reactions, *Am. J. Sci.*, *294*, 529–592, 1994.

Wells, J., D. Janecky, and B. Travis, A lattice gas automata model for hetrogeneous chemical reactions at mineral surfaces and in pore networks, *Physica D*, *47*, 115–123, 1991.

E. Aharonov and M. Spiegelman, Lamont-Doherty Earth Observatory of Columbia University, Palisades, NY 10964. (e-mail: einat@ldeo.columbia.edu; mspieg@ldeo.columbia.edu)

P. Kelemen, Woods Hole Oceanographic Institution, Woods Hole, MA 02543. (e-mail: peterk@cliff.whoi.edu)

(Received June 21, 1996; revised March 25, 1997;
accepted April 2, 1997.)